Indonesian Journal of Chemical Research

http://ojs3.unpatti.ac.id/index.php/ijcr Indo. J. Chem. Res., 12 (1), 16-25, 2024

# Effect on NOx Abatement Performance of Metallic and Bimetallic (Copper and Platinum) Photodeposition onto Anatase $TiO_2$

Chairul Ichsan[1*], Widya Febriani[2]

[1]Department of Chemistry, Faculty of Science and Technology, Universitas Islam Negeri Raden Fatah Palembang. Jl. Pangeran Ratu, 5 Ulu, Kecamatan Seberang Ulu I, Kota Palembang, Sumatera Selatan. 30252, Indonesia
[2]Universitas Negeri Padang. Jl. Prof. Dr. Hamka, Air Tawar Barat, Kecamatan Padang Utara, Kota Padang, Sumatera Barat. 25171, Indonesia
[*]*Corresponding Author: chairulichsan_uin@radenfatah.ac.id*

Received: October 2023
Received in revised: February 2024
Accepted: May 2024
Available online: May 2024

**Abstract**

To enhance the $TiO_2$ anatase's ability to degrade nitrogen oxides (NOx), this study seeks to optimize the photocatalytic activity, selectivity, and DeNOx index of anatase $TiO_2$ nanoparticles through surface modification using metallic and bimetallic (Cu dan Pt) photodeposition. The samples' photocatalytic performance is assessed by NOx abatement measurement, while their characteristics are analyzed using UV-Vis diffuse reflectance and an X-ray diffractometer. According to the measurement, S6 (0.05% $Pt/TiO_2$) has a photonic efficiency of 0.17 for the degradation of NOx, which is 2.15 times higher than bare TiO2. The DeNOx index, which combines selectivity and photonic efficiency, suggests that S9 (0.05% Pt + 0.1% $Cu/TiO_2$) is the most effective sample in the visible light region, with a value of 0.01. Under broadband illumination, S6 has a DeNOx index of 0.13, which is the highest among all samples, while S9 has a moderate-level DeNOx index of 0.019. All samples have a higher DeNOx index than the bare anatase $TiO_2$ nanoparticles. Bimetallic samples exhibit the best performance under visible light, whereas Pt-modified $TiO_2$ anatase performs best in the broadband light range.

*Keywords: Photocatalyst, anatase $TiO_2$, NOx abatement, Photodeposition*

## INTRODUCTION

Air quality issues have significantly increased in recent decades due to widespread industrialization around the world. Multiple industries emit harmful chemicals into the air and water, posing a significant threat to both human beings and the environment. These emissions are known to cause various diseases and contribute to global warming. Nitrogen oxides (NOx), one of the most dangerous forms of air pollution today, are highly reactive and hazardous gases, classified as indirect air contaminants (Brown et al., 2016; Panigrahi et al., 2022; US EPA, 2017). The main NOxes found in the atmosphere are $NO_2$ and NO, with $NO_2$ being more dangerous. At tropospheric levels, $NO_2$ can combine with other molecules to contribute to acid rain (Environmental Protection Agency (EPA), 1999). Ozone in the Earth's lower atmosphere is significantly detrimental to both human health and the environment. It can impair lung capacity and respiratory inflammation, raising concerns about air quality (Simon et al., 2015). In the United States, the primary source of NOx emissions is the power sector, which is responsible for 98 percent of the emissions. The transportation sector contributes 41 percent of these emissions (Brown et al., 2016). The petrochemical industry is extensively linked to significant air pollution. This sector significantly releases contaminants like nitrogen dioxide ($NO_2$) and sulfur dioxide ($SO_2$). These substances can lead to several immediate health consequences, such as lung function impairments, asthma attacks, and respiratory symptoms (Sopian et al., 2016; Weitekamp et al., 2022; Yim et al., 2019).

Effective techniques are necessary to decompose air pollutants, and photocatalysis stands as one such promising approach. Photocatalysis refers to the phenomenon where a semiconductor photocatalyst is used to degrade air pollutants. Examples of commonly used semiconductor photocatalysts include $TiO_2$ (band gap energy: 3.2 eV), $WO_3$ (band gap energy: 2.8 eV), ZnS (band gap energy: 3.6 eV), and $SrTiO_3$ (band gap energy: 3.2 eV). These materials are capable of promoting a wide variety of chemical reactions (Hoffmann et al., 1995). Among metal oxide-based semiconductors, TiO2 holds significant advantages, making it the most promising material for photocatalysis. Its high photocatalytic activity, chemical stability, non-toxicity, and affordability make

it a leading candidate (Danish et al., 2021). Furthermore, the anatase phase of $TiO_2$ exhibits superior performance compared to the rutile and brookite phases (Akpan & Hameed, 2009; Eddy et al., 2023; Wang et al., 2021). ZnO, another photocatalyst with a band gap of around 3.2 eV, demonstrates high photoactivity and finds applications in environmental fields such as air and water pollution control, wastewater treatment, and hazardous waste management (Modares et al., 2022; Ruiz-Hitzky et al., 2019). However, $TiO_2$ offers a significant advantage in practical environmental applications due to its superior stability compared to ZnO, which suffers from incongruent dissolution (Bica & de Melo, 2020; Hoffmann et al., 1995). Therefore, TiO2's favorable properties have led to its widespread use as a semiconductor in environmental applications. The photocatalytic activity of any photocatalyst is influenced by several key factors, including its band gap, surface area, and size distribution (Kharade & Chang, 2020; Y. Zhang & Xu, 2020). These properties can be modified through various techniques to improve both the activity and selectivity of the photocatalyst. Notably, modifications of $TiO_2$ with metals like Pt and Au have shown enhanced photonic efficiency compared to unmodified $TiO_2$ (Malankowska et al., 2020; Sakthivel et al., 2004). Overall, the ability to modify TiO2 significantly improves its photocatalytic efficiency, making it a promising area for continued research.

This work investigated the surface modification of anatase $TiO_2$ nanoparticles with Cu and Pt using metallic and bimetallic photodeposition. This treatment effectively enhanced the photocatalytic activity, selectivity, and DeNOx index for nitrogen oxide (NOx) degradation. Consistent with previous findings, numerous studies have successfully improved the performance of $TiO_2$ through photo deposition modification. One successful example is the photo deposition of copper onto $TiO_2$ (Lennox et al., 2016; Morrison et al., 2009). Photodeposition offers several advantages over other methods, such as impregnation, sputtering, and electroplating. These advantages include superior geometric dispersion and the absence of high temperature and complex setups, requiring only illumination (Morrison et al., 2009; Rizkiana et al., 2020; Tumbel et al., 2015; Wenderich & Mul, 2016). It also requires no high temperatures and is a simple method requiring only illumination (Wenderich & Mul, 2016). Several studies have evaluated the performance of both unmodified and modified $TiO_2$ photocatalysts in degrading NOx, demonstrating the success of both forms in mitigating NOx pollution (Bloh et al., 2014; Meng et al., 2019). Furthermore, studies have found that modifying $TiO_2$ with metals like Fe, Ru, and W can further enhance its performance. The DeNOx index has been established as the most effective method for assessing the effectiveness of $TiO_2$-based photocatalysts in reducing NOx levels (Bloh et al., 2014; L. Yang et al., 2017).

## METHODOLOGY

### Materials

Anatase $TiO_2$/PC105 obtained from CristalACTiV™, $Cu(NO_3)_2 \cdot 2.5H_2O$ with a purity of 99.99% and Methanol purchased from Sigma-Aldrich, as well as Platinart 100 Liquid Pt 4 g/L sourced from EEJA were used for this work without any additional purification.

### Synthesis of Modified Photocatalysts

Nine samples were synthesized in this experiment, with three for each of the three materials. The photo-deposition method used to fabricate the samples was adapted from Wenderich and Mul (2016) with some modifications.

The synthesis process is as follows: 1 mL of methanol, 1 g of $TiO_2$, and a specific precursor are mixed in a centrifuge tube. The mixture is sonicated for homogeneity before being transferred to a container. The container is then placed under a UV lamp and purged with $N_2$ gas while under illumination. After the deposition is complete, the suspension is transferred back to a centrifuge tube and centrifuged. The nanoparticles settle at the bottom, and the supernatant liquid is discarded. The remaining solid sample is then washed three times with deionized water and dried at 80 °C for 18 hours. The dried powder is ground and placed in a small glass flask before being heated at 105 °C in an oven for 3 hours. Finally, the sample is removed from the oven and is ready for measurement.

*Cu Photodeposition onto Anatase $TiO_2$*

A copper(II) nitrate hemi(pentahydrate) precursor with 99.99% purity was used for the photodeposition of the $TiO_2$ photocatalyst. The method employed is similar to the approach described by Lennox et al., 2016. The synthesis was carried out in a beaker covered with thick, opaque black tape to exclude light. To prepare the solution, a mixture of one gram of $TiO_2$, one milliliter of methanol, various concentrations of copper solutions (0.1%, 0.5%, and 1%), and deionized water were combined in a centrifuge tube, resulting in a total volume of approximately 50 milliliters. The mixture was shaken manually and then sonicated in an ultrasonic bath for 10 minutes to achieve homogeneity before being transferred to a prepared container. The

container's top was sealed tightly with a flat borosilicate glass window to allow for UV light transmission. The container was positioned 46 cm from the OSRAM ULTRA-VITALUX 230V UV lamp and irradiated for three hours. Nitrogen gas was continuously purged through the system during irradiation to remove oxygen. Following irradiation, the suspension was centrifuged and washed three times with deionized water.

*Pt Photodeposition onto Anatase $TiO_2$*

Similarly, photo-deposition is employed to prepare Pt-modified $TiO_2$. However, a liquid Pt solution (EEJA's Platinart 100, 4 grams per liter) is used as the precursor in varying proportions (0.005%, 0.01%, and 0.05%). The remaining steps follow the procedure outlined in the previous section.

*Pt-Cu Bimetallic Photodeposition onto Anatase $TiO_2$*

This work employed a modified photodeposition approach for the one-pot synthesis of bimetallic $TiO_2$ photocatalysts, as described by Louis, 2016. Copper(II) nitrate hemi(pentahydrate) ($Cu(NO_3)_2{\cdot}2.5H_2O$) with 99.99% purity (Sigma-Aldrich) and Platinart 100 Liquid Pt 4 g/L (EEJA) served as precursors. A 0.1% copper component formed the core while varying shell percentages of Pt (0.005%, 0.01%, and 0.05%) were used. The Cu-core modified $TiO_2$ was prepared using the previously described Cu photo deposition method onto $TiO_2$. Subsequently, a specific amount of the Pt precursor was added to the mixture, followed by UV irradiation for one hour. Table 1 summarizes the characteristics of all samples.

Table 1. Details of photocatalyst samples

| Samples | Details |
|---|---|
| S1 | 0.1%Cu/$TiO_2$ |
| S2 | 0.5%Cu/$TiO_2$ |
| S3 | 1%Cu/$TiO_2$ |
| S4 | 0.005%Pt/$TiO_2$ |
| S5 | 0.01%Pt/$TiO_2$ |
| S6 | 0.05%Pt/$TiO_2$ |
| S7 | 0.1%Cu + 0.005%Pt/$TiO_2$ |
| S8 | 0.1%Cu + 0.05%Pt/$TiO_2$ |
| S9 | 0.1%Cu + 0.05%Pt/$TiO_2$ |

**NOx Abatement**

The NOx reactor is used to assess the selectivity and activity of the samples, employing a method similar to that of Bloh, Folli, and Macphee (2014), with some modifications. The photocatalytic samples are placed inside a flat, rectangular glass vessel with an area of 0.005 m² within the reactor. The samples (0.2 g) are uniformly distributed on the glass surface. Nitrogen monoxide (NO) is introduced into the reactor and flows through the samples at a rate of 5.10 cc/min. The total volumetric flow rate of the gas stream, accounting for both dry air and humidity, is 1000 cm (1 L/min). The reactor's light source is an Ultra-Vitalux 300W lamp. Figure 1 illustrates the illumination plan for a sample measurement.

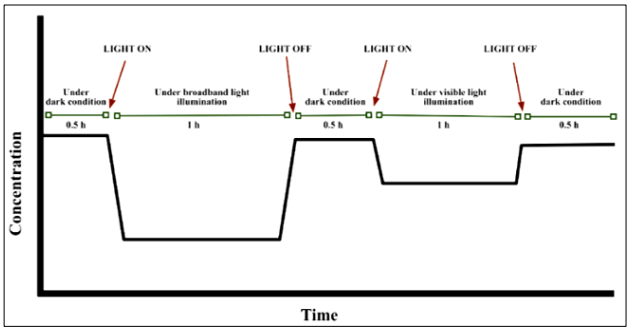


Figure 1. Schematic of sample illumination in NOx reactor

For the first 30 minutes, the samples are kept in the dark. Following this, the samples are exposed to broad-band light for 60 minutes. The light is then turned off, and the samples are left in the dark for 30 minutes before a 420 nm filter is placed on the reactor. Finally, the samples are irradiated with visible light for another hour before being shut down.

With a sufficient amount of light energy, the reaction that takes place in the reactor can be described as follows:

$$NO\bullet \xrightarrow{\bullet OH} HONO \xrightarrow{\bullet OH} NO_2\bullet \xrightarrow{\bullet OH} HONO_2\ (NO_3^-)$$

The outlet gas from the reactor is analyzed with a Thermo Scientific Model 42i-HL High-Level NO-$NO_2$-NOx Analyzer (Air Monitors Ltd., UK) for measuring NO, $NO_2$, and NOx levels. This monitored data allows for calculations of photonic efficiency, selectivity, and DeNOx index.

**Characterisation**

*UV/Vis Diffuse Reflectance Spectroscopy*

This method of characterizing photocatalysts uses the Agilent Cary 60 UV-Vis spectrophotometer in the diffuse reflectance setting with $BaSO_4$ as the internal benchmark. For each sample, its band gap can be calculated using either the Tauc plot or the Kubelka-Munk function plot. Equation 1 provides the input data for the Tauc plot.

$$[F(R_\infty)(hv)]^{\frac{1}{j}} = B(hv - E_g] \qquad (1)$$

(Kisch, 2015; Murphy, 2007; Praveen et al., 2014)

The Kubelka-Munk function (F(R∞)), depicted on the y-axis, and the band gap (Eg), on the x-axis, were utilized in this study. The semiconductor employed was $TiO_2$ anatase with an indirect bandgap and a value of 2 for the diffusion length j.

*X-Ray Diffractometer*

XRD spectra are characterized using a Phillips X-ray diffractometer equipped with Cu Kα radiation (λ = 0.15418 nm). These studies were aimed at identifying crystal phase composition and measuring crystallite size. The crystallite size is calculated using the Debye-Scherrer equation as shown in Equation 2.

$$d = \frac{k\lambda}{(\beta cos\theta)} \quad (2)$$

(Bindu & Thomas, 2014; Jacob et al., 2014; X. Yang et al., 2015)

The Scherrer constant corresponds to a value of 0.94 for the constant k for the experiment performed with anatase $TiO_2$.

## RESULTS AND DISCUSSION

### NOx Abatement in NOx Reactor

In the NOx reactor, unmodified $TiO_2$, the anatase $TiO_2$ used in this study, and $TiO_2$ photo-modified by Cu and Pt photodeposition are evaluated for NO and $NO_2$ removal efficiency under broadband and visible irradiance. Figure 2 shows photocatalytic efficiencies of all samples degrading NOx in darkness and for 1 hour under broadband and visible irradiance.

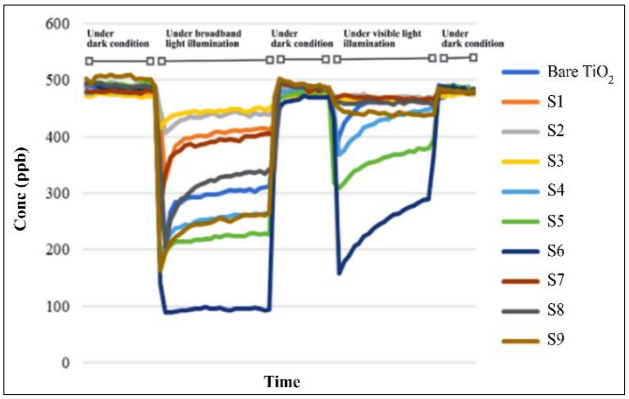


Figure 2. NOx Abatement of All Samples

Of all the samples, S6 has the highest percentage of metallic platinum (Pt)/$TiO_2$. This sample shows significant NOx reduction under both broadband and visible light exposure, reducing the NO level from 0.5 ppm to just over 0.1 ppm under broadband irradiance. On the other hand, S3 with 1% Cu deposited on the surface of anatase $TiO_2$ has the worst NO removal behavior, achieving only approximately 0.44 ppm under broadband radiation. Only four samples show better performance under broadband irradiance even compared to bare anatase $TiO_2$: S4, S5, S6, and S9. Compared to bare anatase $TiO_2$, all $TiO_2$ samples with photodeposited Cu on the surface show inferior activity.

The monitoring of the concentrations of $NO_2$ and NO in the reactor, under different conditions such as broadband and visible light, dry or humid air, is used to determine the degradation of NOx. In terms of degradation of NO and NOx, the Cu-supported anatase $TiO_2$ samples show a significant tendency compared to the Pt and Cu-Pt supported anatase $TiO_2$ samples. The concentration of Cu on anatase $TIO_2$ shows an inverse relationship with its ability to degrade NO and NOx. The S1 variant of 0.1% Cu/$TiO_2$ shows the highest efficiency among the other variants. As shown in Figure 3, the NO degradation performance is higher in the Pt/$TiO_2$ and Cu-Pt/$TiO_2$ samples with higher Pt concentrations.

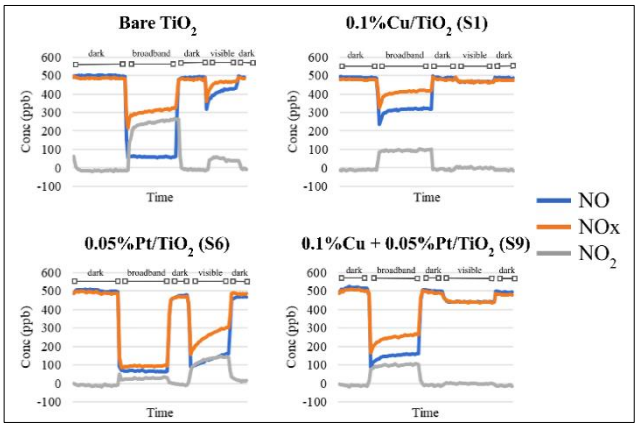


Figure 3. NOx, NO, and $NO_2$ Abatement of Bare anatase $TiO_2$, S1, S2 and S9

Under broadband light, it is evident that S6 outperforms other samples because it significantly degrades NO and generates only small amounts of $NO_2$. In contrast, the performance of bare anatase $TIO_2$, while degrading a great deal of NO, produces a significant amount of NO2, a known toxicant with a low limit of 1 to 3 ppm compared to the 25 ppm limit of NO. S6 is superior in reducing NO from 0.5 ppm to 0.3 ppm in the visible range. However, when it comes to $NO_2$ generation, S9 is the optimal sample since it barely produces any $NO_2$.

### *Performance under the Broadband Light Irradiation*

The photonic efficiency (ξ) measures the degradation of the molecules about the number of photons that impinge upon them. Its calculation is expressed by the following equation:

$$\xi = \frac{(C_d - C_i)Vp}{\phi ART} \quad (3)$$

(MacPhee & Folli, 2016)

Photonic efficiency (ξ) quantifies a molecule's photocatalytic activity and can inform its performance. Employing photonic efficiency (ξ) provides a measurable means of evaluating effectiveness.

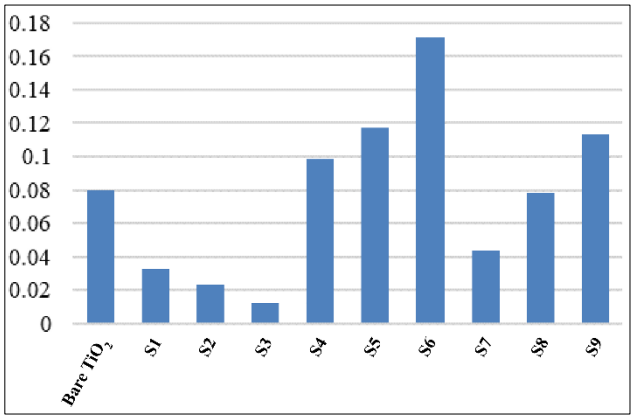


Figure 4. Photonic Efficiency of NOx under the Broadband Light Irradiation

Figure 4 presents the varied trends in photocatalytic activity observed for Cu/$TiO_2$ samples under broad-band light irradiation. Samples S1, S2, and S3 contain increasing Cu concentrations of 0.1%, 0.5%, and 1%, respectively. The results show that increasing the Cu content leads to a decrease in photocatalytic activity. Notably, sample S3 exhibits the lowest photonic efficiency, with a value below 0.02.

In contrast, both Pt/$TiO_2$ samples (S4, S5, and S6) and Cu-Pt/$TiO_2$ samples (S7, S8, and S9) exhibit an upward trend in photonic efficiency when exposed to broad-band light. Interestingly, Pt/$TiO_2$ displays the most remarkable effect in enhancing the efficiency of anatase $TiO_2$.

While $TiO_2$ and its modified photocatalysts effectively degrade NO to $NO^{3-}$, $NO_2$ is initially generated as an intermediate before complete conversion. Notably, $NO_2$ possesses a significantly higher negative impact on health compared to NO and is therefore undesirable. An effective photocatalyst should demonstrate the ability to degrade NO efficiently despite the presence of $NO_2$. Photonic efficiency, although a useful measure of individual performance for NO or $NO_2$, does not account for the overall conversion pathway.

Selectivity is a crucial factor in evaluating photocatalysts. Ideally, a photocatalyst should effectively convert almost all NO into the non-harmful product, nitrate ($NO^{3-}$), before releasing any $NO_2$ or NO into the atmosphere. The percentage of selectivity can be calculated using the following equation:

$$S = \frac{\xi NOx}{\xi NO} \quad (4)$$

(MacPhee & Folli, 2016)

Different variations in selectivity (%) under broad-spectrum light irradiation are demonstrated in Figure 5. Compared to the photonic efficiency of all samples under broadband light exposure, the selectivity (%) values show relatively similar trends, and the metal concentrations show a direct correlation with the selectivity (%).

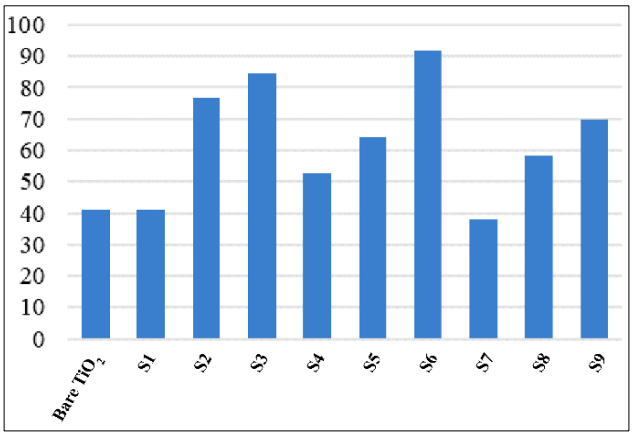


Figure 5. Selectivity (%) under the Broadband Light Irradiation

S1, S2, and S3 display higher selectivity (%) than their photonic efficiency performance, as they produce fewer harmful molecules by reducing the formation of $NO_2$ (refer to Figure 2). According to Figure 5, the majority of samples exhibit higher selectivity (%) compared to bare anatase $TiO_2$, while the rest show similar selectivity (%) levels to that of bare anatase $TiO_2$, which is around 40%.

***Performance under the Visible Light Irradiation***

A significant difference in the photonic efficiency and selectivity in the visible region compared to that in the broadband light region can be seen in Figures 6 and 7. Pt anatase $TIO_2$ samples (S4, S5, and S6) showed a significant improvement in photocatalytic activity under visible light exposure, as reflected in photonic efficiency values. Especially S6 reached about 0.10, ten times better than the bare antase $TiO_2$ that only reached 0.01.

The selectivity percentage under visible light illumination demonstrates significant variability (refer to Figure 7). All samples exhibit higher selectivity than bare anatase $TiO_2$. In comparison to other sample types (Cu anatase $TiO_2$ and Cu-Pt/$TiO_2$), the selectivity percentage of $TIO_2$ is relatively lower. However,

Cu/$TiO_2$ samples (S1, S2, and S3) exhibit higher selectivity percentages than other samples.

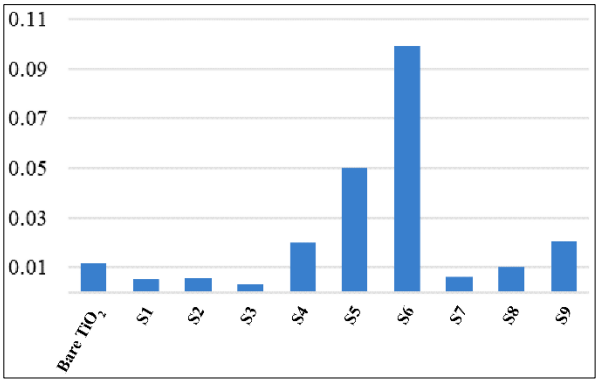


Figure 6. Photonic Efficiency of NOx under Visible Light

In terms of photocatalytic efficiency and selectivity (%), the Cu-Pt anatase $TiO_2$ samples show a consistent trend and position themselves at a moderate level under all types of light irradiation. The selectivity and photocatalytic efficiency of these samples are not excessively low; on the contrary, they are either high or moderate.

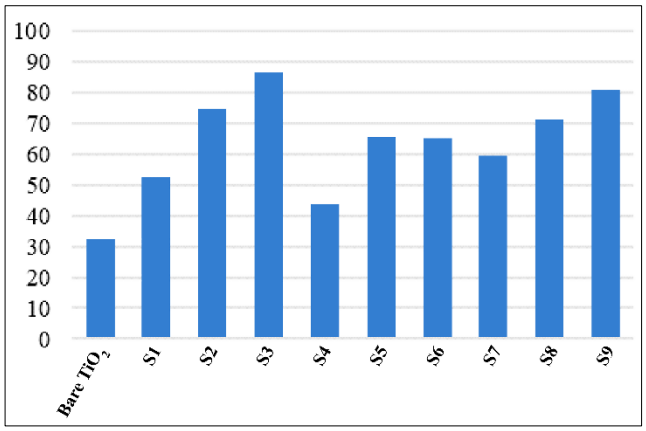


Figure 7. Selectivity (%) under Visible Light

### *DeNOx Index of Samples*

The DeNOx Index is a measure that evaluates activity by considering both photonic efficiency (ξ) and selectivity (S). Its calculation utilizes the following formula.

$$\xi DeNOx = \xi NO - 3\xi NO_2 \quad (5)$$

$$\xi DeNOx = \xi NOx \left(3 - \frac{2}{S}\right) \quad (6)$$

(MacPhee & Folli, 2016)

The DeNOx index provides a toxicity assessment for both NO and $NO_2$ to improve measurement efficiency by avoiding reliance on single nitrogen oxide values. Table 2 shows the DeNOx index of both the unmodified and the modified anatase $TiO_2$ samples used in this study.

Table 2. DeNOx Index of Samples under Broadband and Visible Light Irradiation

| DeNOx Indeks | | |
|---|---|---|
| Samples | Broadband Irradiation | Visible Irradiation |
| Bare $TiO_2$ | -0.149 | -0.036 |
| S1 | -0.060 | -0.004 |
| S2 | 0.009 | 0.002 |
| S3 | 0.008 | 0.002 |
| S4 | -0.079 | -0.032 |
| S5 | -0.013 | -0.002 |
| S6 | 0.140 | -0.007 |
| S7 | -0.098 | -0.002 |
| S8 | -0.033 | 0.002 |
| S9 | 0.016 | 0.011 |

The DeNOx index is a dimensionless value. It can be either positive or negative. A positive reading means that overall NOx toxicity is decreasing, while a negative reading means that toxicity is increasing. To understand how the samples differ, see the bar graphs shown in Figures 8 and 9.

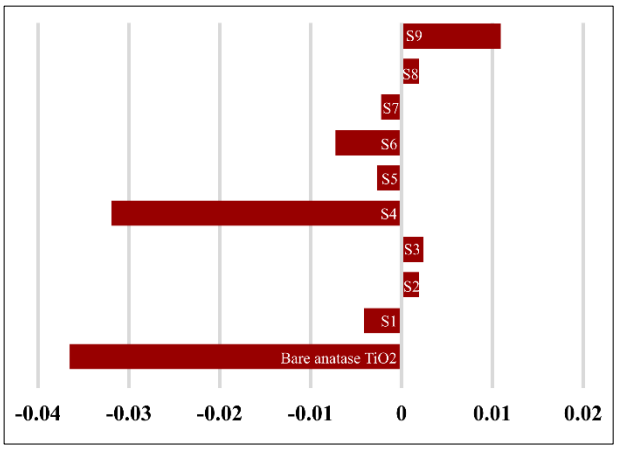


Figure 8. DeNOx Index of Samples under Broadband Light Irradiation

In the broad spectrum of light, S6 displays a markedly higher DeNOx index than the other samples, measuring 0.14. S9 closely follows at 0.016 DeNOx index. All samples, which outperform the bare anatase $TiO_2$, demonstrate superior DeNOx indices. The bare anatase $TiO_2$ features a DeNOx index of -0.149. This phenomenon occurs because naked TiO2 generates a

greater quantity of $NO_2$ when exposed to broadband light irradiation, resulting in noticeably higher toxicity than NO (Martinez-Oviedo et al., 2021; Witkowski et al., 2022; L. Yang et al., 2017). This generates roughly 0.28 ppm of NO2 from 0 ppm (see Figure 2).

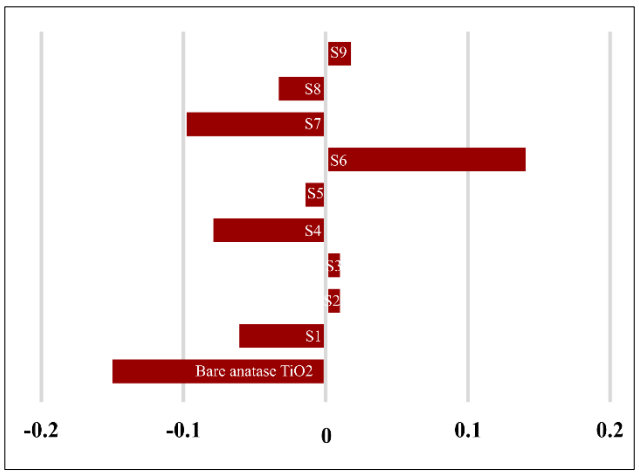


Figure 9. DeNOx Index of Samples under Visible Light Irradiation

Likewise, within the visible light spectrum, unmodified anatase $TiO_2$ exhibits a lower DeNOx index compared to the modified anatase $TiO_2$ samples. Sample S9, which ranks second in performance across a range of wavelengths, achieves the highest DeNOx Index under visible light irradiation, measured at 0.011. Sample S6, which has the highest DeNOx Index among different wavelengths, shows a negative score of -0.007 under visible light exposure, which means an increase in overall toxicity.

S9 (0.1% Cu + 0.05% Pt/$TiO_2$) is the top-performing photocatalyst in the visible region with regard to the DeNOx Index. While this research shows that its selectivity and photonic efficiency are only moderately effective under visible region illumination, it produces lower levels of $NO_2$ than the other samples, thus creating fewer harmful compounds. Reducing $NO_2$ is necessary to achieve a higher DeNOx index and decrease the amount of $NO_2$ as it negatively impacts the index.

## Characterisation of Photocatalyst

### UV/Vis Diffuse Reflectance

Figure 10 depicts the Kubelka-Munk function F(R∞) plots of various samples and bare anatase $TiO_2$. The band gap is determined by analyzing the Kubelka-Munk function F(R∞) (Utomo & Wihadi, 2022) plot (Equation 1).

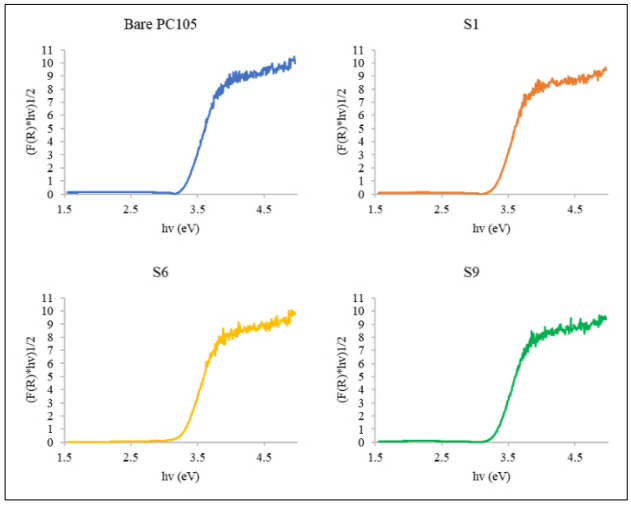


Figure 10. Bare anatase $TiO_2$, S1, S6, and S9 taut plots

Figure 10 displays examples of each sample type used in the experiment. S1 and S6 represent samples prepared by the photodeposition of Cu and Pt, respectively, onto anatase $TiO_2$. In contrast, S9 exemplifies the bimetallic photodeposition of Cu and Pt onto bare anatase $TiO_2$. Table 3 shows that the band gap values of all samples are relatively similar. Additionally, Figure 10 demonstrates the absence of metal oxide deposition on the surface of anatase TiO2. This is further supported by the lack of several characteristic absorption peaks at various wavelengths in the Tauc plot (Figure 10). These findings suggest that the deposited substances on anatase $TiO_2$ are metallic, consisting of Cu, Pt, or a combination of both. If PtO or CuO were deposited on the surface of anatase $TiO_2$, the Tauc plot would exhibit two distinct peak types located at different bandgaps. This is because the band gaps of PtO and CuO are smaller than those of $TiO_2$-based semiconductors (Hu et al., 2015; X. Zhang & Tang, 2012).

Table 3. Bandgap values of samples

| Samples | Bandgap |
|---|---|
| Bare anatase $TiO_2$ | 3.28 |
| S1 | 3.27 |
| S2 | 3.27 |
| S3 | 3.23 |
| S4 | 3.26 |
| S5 | 3.25 |
| S6 | 3.25 |
| S7 | 3.26 |
| S8 | 3.26 |
| S9 | 3.26 |

### X-ray diffractometer (XRD)

XRD is utilized to measure the grain size and phase of the materials. Figure 11 displays the XRD spectra derived from the analysis of the samples conducted throughout this research. All peaks in the spectra of the samples have similar 2θ positions. The six most intense peaks are located at approximately 25.34, 37.83, 48.15, 53.93, 55.1, and 62.95 2θ positions.

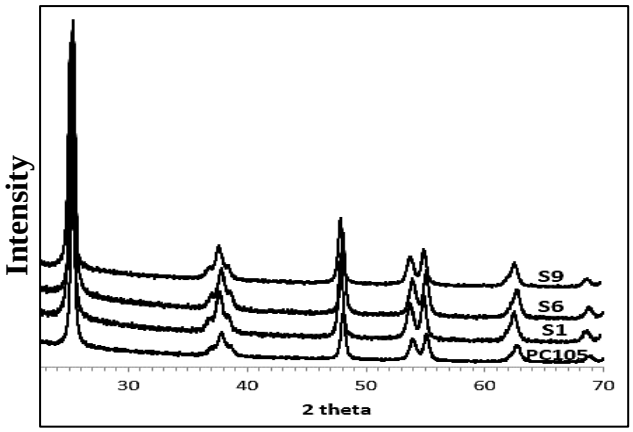


Figure 11. XRD Spectra of Unmodified and Modified $TiO_2$ Samples

In the XRD spectra (Figure 11), the metals (Cu and Pt) deposited on anatase $TiO_2$ are not visible. A possible reason is that the metal concentration used in this study is too low for XRD detection (Holder & Schaak, 2019; Stanjek, 2004). Furthermore, the surface modification of anatase $TiO_2$ is investigated in this study, which leads to the assumption that crystallite size is not significantly different. The results in Figure 12 show that the mean crystal size for all samples, including bare TiO2, is around 12.1 nm.

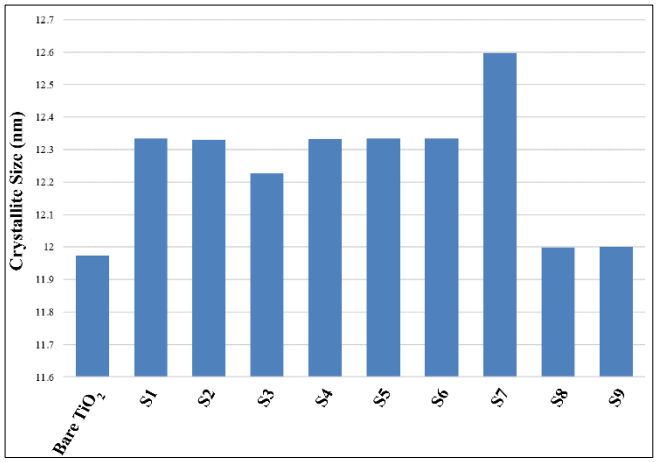


Figure 12. Crystallite Size of Samples (nm)

## CONCLUSION

The photo-deposition method successfully synthesized anatase $TiO_2$ with improved photocatalytic performance in several samples. This indicates that the metal deposits as a pure metal, not as metal oxide, according to the UV-Vis diffuse reflectance data for all modified samples. All modified samples exhibit superior photocatalytic performance compared to bare anatase $TiO_2$ in terms of the DeNOx index. Bimetallic-modified photocatalysts demonstrate optimal performance in the visible region, while Pt-modified anatase $TiO_2$ shows superior efficiency under broadband radiation. Among the modified samples, S9 (0.05% Pt + 0.1% Cu/$TiO_2$) achieved the highest DeNOx index (0.01) in the visible light range, indicating its superior selectivity and photonic efficiency. However, under broadband illumination, S6 exhibited the highest DeNOx index (0.13), while S9 had a moderate value of 0.019. This suggests a trade-off between selectivity and light utilization. In terms of photonic efficiency for NOx degradation under broadband light, S6 displayed the highest value (0.17) with 0.05% Pt deposited, which is 2.15 times higher than that of bare $TiO_2$. Notably, S6 also exhibited the highest photonic efficiency (0.09) among the modified samples in the visible region. However, the lower DeNOx index of S6 under broadband illumination compared to S9 suggests that Pt-modified samples might produce more the harmful $NO_2$ gas. X-ray diffraction (XRD) and ultraviolet-visible diffuse reflectance spectroscopy (UV-Vis DRS) characterization revealed no significant changes in crystallite size (averaging around 12 nm) or band gap (averaging around 26 nm).

## ACKNOWLEDGMENT

I would like to acknowledge Dr. Amer Hakki for his guidance on the theoretical aspects of my research. I would also like to thank the team at the University of Aberdeen and UIN Raden Fatah Chemistry Laboratories for supporting me with the practical aspects of this research.

## REFERENCES

Akpan, U. G., & Hameed, B. H. (2009). Parameters affecting the photocatalytic degradation of dyes using TiO2-based photocatalysts: A review. *Journal of Hazardous Materials*, *170*(2–3), 520–529.

Bica, B. O., & de Melo, J. V. S. (2020). Concrete blocks nano-modified with zinc oxide (ZnO) for photocatalytic paving: Performance comparison with titanium dioxide (TiO2). *Construction and*

*Building Materials*, *252*, 119120.

Bindu, P., & Thomas, S. (2014). Estimation of lattice strain in ZnO nanoparticles: X-ray peak profile analysis. *Journal of Theoretical and Applied Physics*, *8*(4), 123–134.

Bloh, J. Z., Folli, A., & Macphee, D. E. (2014). Photocatalytic NOx abatement: Why the selectivity matters. *RSC Advances*, *4*(86), 45726–45734.

Brown, P., Broomfield M, Buys G, Cardenas, L., Kilroy E, MacCarthy J, Murrells T, Pang Y, Passant N, Ramirez Garcia J, Thistlethwaite G, & Webb N. (2016). UK Greenhouse Gas Inventory, 1990 to 2014. Annual Report for Submission under the Framework Convention on Climate Change. In *Science Research Programme of the Department of Energy and Climate Change.* (Issue April).

Danish, M. S. S., Estrella, L. L., Alemaida, I. M. A., Lisin, A., Moiseev, N., Ahmadi, M., Nazari, M., Wali, M., Zaheb, H., & Senjyu, T. (2021). Photocatalytic applications of metal oxides for sustainable environmental remediation. *Metals*, *11*(1), 1–25.

Eddy, D. R., Permana, M. D., Sakti, L. K., Sheha, G. A. N., Solihudin, G. A. N., Hidayat, S., Takei, T., Kumada, N., & Rahayu, I. (2023). Heterophase Polymorph of TiO2 (Anatase, Rutile, Brookite, TiO2 (B)) for Efficient Photocatalyst: Fabrication and Activity. *Nanomaterials*, *13*(4).

Environmental Protection Agency (EPA). (1999). Nitrogen oxides (NOx), why and how they are controlled. *Epa-456/F-99-006R*, *November*, 48. https://doi.org/EPA 456/F-99-006R

Hoffmann, M. R., Martin, S., Choi, W., & Bahnemann, D. W. (1995). Environmental Applications of Semiconductor Photocatalysis. *Chemical Reviews*, *95*(1), 69–96.

Holder, C. F., & Schaak, R. E. (2019). Tutorial on Powder X-ray Diffraction for Characterizing Nanoscale Materials. *ACS Nano*, *13*(7), 7359–7365.

Hu, Y., Song, X., Jiang, S., & Wei, C. (2015). Enhanced photocatalytic activity of Pt-doped TiO2 for NOx oxidation both under UV and visible light irradiation: A synergistic effect of lattice Pt4+ and surface PtO. *Chemical Engineering Journal*, *274*(x), 102–112.

Jacob, R., Nair, H. G., & Isac, J. (2014). Structural and Morphological Studies of Nanocrystalline Ceramic. *International Letters of Chemistry, Physics and Astronomy*, *41*, 100–117.

Kharade, A. K., & Chang, S. M. (2020). Contributions of Abundant Hydroxyl Groups to Extraordinarily High Photocatalytic Activity of Amorphous Titania for CO2Reduction. *Journal of Physical Chemistry C*, *124*(20), 10981–10992.

Kisch, H. (2015). *Semiconductor Photocatalysis: Principles and Applications*. Wiley-VCH Verlag GmbH & Co. KGaA. https://doi.org/10.1002/9783527673315.ch1

Lennox, A. J. J., Bartels, P., Pohl, M. M., Junge, H., & Beller, M. (2016). In situ photodeposition of copper nanoparticles on TiO2: Novel catalysts with facile light-induced redox cycling. *Journal of Catalysis*, *340*, 177–183.

Louis, C. (2016). Chemical Preparation of Supported Bimetallic Catalysts. Gold-Based Bimetallic, a Case Study. *Catalysts*, *6*(8), 110.

MacPhee, D. E., & Folli, A. (2016). Photocatalytic concretes - The interface between photocatalysis and cement chemistry. *Cement and Concrete Research*, *85*, 48–54.

Malankowska, A., Mikołajczyk, A., Mędrzycka, J., Wysocka, I., Nowaczyk, G., Jarek, M., Puzyn, T., & Mulkiewicz, E. (2020). The effect of Ag, Au, Pt, and Pd on the surface properties, photocatalytic activity, and toxicity of multicomponent TiO2-based nanomaterials. *Environmental Science: Nano*, *7*(11), 3557–3574.

Martinez-Oviedo, A., Kshetri, Y. K., Joshi, B., & Lee, S. W. (2021). Surface modification of blue TiO2 with silane coupling agent for NOx abatement. *Progress in Natural Science: Materials International*, *31*(2), 230–238.

Meng, A., Zhang, L., Cheng, B., & Yu, J. (2019). Dual Cocatalysts in TiO2 Photocatalysis. *Advanced Materials*, *31*(30), 1–31.

Modares, M., Alijani, S., & Nasernejad, B. (2022). NOx photocatalytic degradation over ZnO–CdS heterostructure composite under visible light irradiation. *Research on Chemical Intermediates*, *48*(5), 1831–1845.

Morrison, E., Gutiérrez-Tauste, D., Domingo, C., Vigil, E., & Ayllón, J. A. (2009). One step room temperature photodeposition of Cu/TiO2 composite films and its conversion to CuO/TiO2. *Thin Solid Films*, *517*(19), 5621–5624.

Murphy, A. B. (2007). Band-gap determination from diffuse reflectance measurements of semiconductor films, and application to photoelectrochemical water-splitting. *Solar Energy Materials and Solar Cells*, *91*(14), 1326–1337.

Panigrahi, T. H., Sahoo, S. R., Murmu, G., Maity, D.,

& Saha, S. (2022). Current challenges and developments of inorganic/organic materials for the abatement of toxic nitrogen oxides (NOx) – A critical review. *Progress in Solid State Chemistry*, *68*, 100380.

Praveen, P., Viruthagiri, G., Mugundan, S., & Shanmugam, N. (2014). Structural, optical, and morphological analyses of pristine titanium di-oxide nanoparticles - Synthesized via sol-gel route. *Spectrochimica Acta - Part A: Molecular and Biomolecular Spectroscopy*, *117*, 622–629.

Rizkiana, J., Suyadi, A. F., Auliardi, D., Devianto, H., & Soerawidjaja, T. H. (2020). Photocatalyst Characterization for Photoreduction of Carbon Dioxide to Produce Formic Acid in Aquatic. *Indo. J. Chem. Res.*, *8*(1), 35–42. https://doi.org/10.30598/10.30598//ijcr.2020.8-jen

Ruiz-Hitzky, E., Aranda, P., Akkari, M., Khaorapapong, N., & Ogawa, M. (2019). Photoactive nanoarchitectures based on clays incorporating TiO2 and ZnO nanoparticles. *Beilstein Journal of Nanotechnology*, *10*, 1140–1156.

Sakthivel, S., Shankar, M. V., Palanichamy, M., Arabindoo, B., Bahnemann, D. W., & Murugesan, V. (2004). Enhancement of photocatalytic activity by metal deposition: Characterisation and photonic efficiency of Pt, Au, and Pd deposited on TiO2 catalyst. *Water Research*, *38*(13), 3001–3008.

Simon, H., Reff, A., Wells, B., Xing, J., & Frank, N. (2015). Ozone trends across the United States throughout decreasing NOx and VOC emissions. *Environmental Science and Technology*, *49*(1), 186–195.

Sopian, N. A., Jalaludin, J., Bahri, S., & Tamrin, M. (2016). *Risk of Respiratory Health Impairment among Susceptible Population Living Near Petrochemical Industry - A Review Article*. *45*(1), 9–16.

Stanjek, H. H. W. (2004). Basics of X-Ray Diffraction. *Hyperfine Interactions*, *154*, 107–119. https://doi.org/10.1023/B:HYPE.0000032028.60546.38

Tumbel, E. D., Wuntu, A. D., & Abidjulu, J. (2015). Photodegration of Remazol Yellow Using A-Type Zeolite/TIO2. *Indonesian Journal of Chemical Science*, *3*, 238–241.

US EPA. (2017). *Nitrogen Oxides (NOx) Control Regulations*.

Utomo, A. D. C., & Wihadi, M. N. K. (2022). Preparation of ZnO/TiO2 Nanocomposite Sensitized Mangosteen Rind (Garcinia mangostana L) Dye for Light Harvesting Efficiency in Solar Cell. *Indonesian Journal of Chemical Research*, *10*(2), 68–73.

Wang, A., Wu, Q., Han, C., Yang, H., & Xue, X. (2021). Significant influences of crystal structures on photocatalytic removal of NOx by TiO2. *Journal of Photochemistry and Photobiology A: Chemistry*, *407*(August 2020), 113020.

Weitekamp, C. A., Stevens, T., Stewart, M. J., Bhave, P., & Gilmour, M. I. (2022). Health effects from freshly emitted versus oxidatively or photochemically aged air pollutants. *EPA Public Access*.

Wenderich, K., & Mul, G. (2016). Methods, Mechanism, and Applications of Photodeposition in Photocatalysis: A Review. *Chemical Reviews*, *116*(23), 14587–14619.

Witkowski, H., Jackiewicz-Rek, W., Jarosławski, J., Chilmon, K., & Szkop, A. (2022). Ozone Formation during Photocatalytic Oxidation of Nitric Oxides under UV Irradiation with the Use of Commercial TiO2 Photocatalytic Powders. *Materials*, *15*(17).

Yang, L., Hakki, A., Wang, F., & Macphee, D. E. (2017). Different Roles of Water in Photocatalytic DeNOx Mechanisms on TiO2: Basis for Engineering Nitrate Selectivity? *ACS Applied Materials and Interfaces*, *9*(20), 17034–17041.

Yang, X., Wang, S., Sun, H., Wang, X., & Lian, J. (2015). Preparation and photocatalytic performance of Cu-doped TiO2 nanoparticles. *Transactions of Nonferrous Metals Society of China*, *25*(2), 504–509.

Yim, S. H. L., Wang, M., Gu, Y., Yang, Y., Dong, G., & Li, Q. (2019). Effect of Urbanization on Ozone and Resultant Health Effects in the Pearl River Delta Region of China. *Journal of Geophysical Research: Atmospheres*, *124*(21), 11568–11579.

Zhang, X., & Tang, A. (2012). Novel CuO/TiO2 nanocomposite films with a graded band gap for visible light irradiation. *Materials Express*, *2*(3), 238–244.

Zhang, Y., & Xu, X. (2020). Machine Learning Band Gaps of Doped-TiO2Photocatalysts from Structural and Morphological Parameters. *ACS Omega*, *5*(25), 15344–15352.